UV phototransistors based upon spray coated and sputter deposited ZnO TFTs

Dinesh Kumar[1]*, Tiago Carneiro Gomes[1,2], Neri Alves[2], Lucas Fugikawa Santos[3], Graham C. Smith[4] and Jeff Kettle[1]

[1]*School of Electronics, Bangor University, Bangor, Gwynedd, LL57 1UT, Wales, UK.*
[2]*São Paulo State University (Unesp), School of Technology and Sciences, Presidente Prudente, Brazil.*
[3]*São Paulo State University (Unesp), Institute of Geosciences and Exact Sciences, Rio Claro, Brazil*
[4]*Faculty of Science & Engineering, University of Chester, Chester CH2 4NU, UK*

***Abstract*— A comparison of Zinc Oxide (ZnO) phototransistors prepared by spray and sputter coating process is presented. The work shows that spray coated layers provide significant advantages in sensor response over ZnO phototransistors made by physical vapour deposition and we show that spray deposited ZnO phototransistors can exhibit state-of-the-art performances for UV photodetectors. Topographic images of the samples surface shows that there is increase in surface roughness in spray coated samples indicating increasing grain sizes, which is considered the source of the greater sensor responsivity. X-ray photoelectron spectroscopy (XPS) is also used to understand the root cause of the greater UV responsivity. It was observed that sprayed ZnO TFTs are more sensitive to UV radiation due to higher adsorption of oxygen level. Responsivity and external quantum efficiency (EQE) of the sprayed and sputtered ZnO TFTs are also evaluated.**

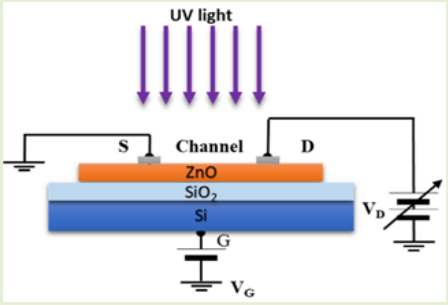

***Key words*— Flexible, ZnO, spray coating, Radio frequency sputtering, detector, TFT, ultraviolet light.**

I. Introduction

ZnO and its compounds have generated significant attention since one of their early reports by Nomura et al. in 2004 [1]–[4]. Due to their outstanding electrical properties, such as high field-effect mobility, good uniformity and low temperature processability, ZnO Thin Film Transistors (TFTs) have potential in a wide range of electronic applications like photodetectors, backplanes for displays and smart packaging [5]–[7]. In terms of sensor behaviour, Anthopoulos et al. demonstrated solution-processed dye-sensitized ZnO phototransistors with high photoresponsivity on the order of 10^4 A/W [8]. Nae-Eung Lee et al reported flexible ultraviolet phototransistor using hybrid channel of vertical ZnO nanorods and graphene showing high-photovoltage responsivity of 10^8 V/W [9]. The benefit of ZnO TFTsas phototransistors, in comparison to photodiodes, is that multiple parameters change on exposure to UV radiation including threshold voltage, mobility and drain ON current. However, in two terminal devices, fewer parameters change giving reduced specificity. In addition, TFTs with tunable threshold voltage, V_{th}, is of particularly high importance for chemical, gas and biological detectors [10].

An earlier version of this paper was presented at the FLEPS 2019 (for link please see footnote[1]) and was published in its proceedings. Here, we are extending the paper and it is shown that the photo-transistors UV detector produced by spray pyrolysis are much more responsive and suited for sensor applications, primarily as a result of their greater responsivity to UV radiation.

In this work, ZnO TFTs have been used as UV photo detectors. ZnO is an established candidate for UV detectors because it has a wide band gap of 3.37 eV [11][12], which corresponds to the UV spectrum. The ZnO active layer conductivity is extremely sensitive to UV radiation exposure, which is related with its photosensitivity regulated by chemisorption of oxygen [13]–[15]. Oxygen molecules can be adsorbed on the surface of ZnO films, resulting in negatively charged oxygen ions that create an electron depletion layer, in which the ZnO layer becomes less conductive near the surface [16]. This chemical process behind this transition is shown below.

$$O_2(g) + e^- \rightarrow O_2^-(ads)$$

$$O_2(g) + 2e^- \rightarrow O_2^{2-}(ads)$$

The interaction between UV radiation and ZnO films generates electron-hole pairs within the ZnO. If the photogenerated hole combines with adsorbed oxygen ions at the ZnO surface, oxygen molecules are regenerated. These can combine with free electrons, thus increasing the conductivity within the of depletion layer of the device [17], [18].

$$h\nu + O_2^-(ads) + h^+ \rightarrow O_2(g)$$
$$h\nu + O_2^{-2}(ads) + 2h^+ \rightarrow O_2(g)$$

[1] https://ieeexplore.ieee.org/document/8792244

In the dark, oxygen is reabsorbed on the surface until the equilibrium is restored again. This desorption process is relatively slow and significantly increases the relaxation time constant of ZnO devices [19]. The use of ZnO in UV photo detection has been well established, however, the optimisation in respect to the material deposition technique is not fully understood. In this paper, we show how the responsivity is enhanced by modifying the photo active layer structurally through different deposition techniques.

II. Experimental

Spray coating deposition was undertaken using an airbrush nozzle actuated by a micro-controlled servomotor to spray a zinc acetate di-hydrated (3% w/w, in methanol) solution onto pre-heated (300ºC) substrates. The substrate heating promotes the solvent evaporation as the solution spray reaches the substrate surface and cause the zinc acetate pyrolysis and subsequent formation of a thin ZnO layer. Spray coating was performed at air pressure of 0.7 bar and the nozzle was kept 20 cm distance from the substrate on hotplate. The resulting ZnO films obtained by this deposition procedure were inspected and highly uniform; with an average thickness of 20 nm. The active layer thickness was determined by Dektak surface profilometer.

ZnO TFTs were also manufactured by using radio frequency (RF) sputtering technique at 75W and 1.2×10^{-2} mbar base pressure. The 99.99% pure ZnO target was pre-sputtered under closed shutter conditions for 5 min to eliminate any surface contaminants. A low sputter rate of 0.05 nm/s was used for the best uniformity. The ZnO layer thickness during deposition by sputtering was monitored with pre-installed thickness detector. For both sets of devices, the source drain contacts were thermally evaporated using Leybold thermal evaporator with 80nm of Aluminium (Al) metal.

For all measurements of ZnO TFTs, the electrical properties I_{on}, I_{off}, I_{on}/I_{off} ratio and mobility were extracted from transfer characteristics of TFT using equations (1) and (2).

$$I_{DS} = \mu C_i \frac{W}{2L}(V_{GS} - V_{th})^2 \quad (1)$$

$$\mu_{sat} = \left(\frac{\partial\sqrt{I_D}}{\partial V_G}\right)^2 \frac{2L}{WC_i} \quad (2)$$

where, W is channel width and L is channel length, C_i is dielectric capacitance, μ is carrier mobility, V_G applied gate voltage, V_D is drain voltage, and V_{th} is the TFT threshold voltage.

For UV saturation experiments, the ZnO TFTs were placed on a temperature controlled hot plate and UV light was illuminated onto the TFT using UV-LEDs with wavelengths of 355nm, 365nm and 370nm, purchased from Roithner Laser technik Austria. The TFTs were exposed to UV light for 5 minutes and transfer characteristics of TFT were measured before and after UV exposure. Measurements were performed at different substrate temperatures and the irradiance (0.214 mW/mm^2) was controlled and measured during the.

The XPS data were acquired using a bespoke UHV system fitted with a Specs GmbH Focus 500 monochromated Al Kα X-ray source made by Specs GmbH. Survey spectra were acquired over the binding energy range 1100–0 eV using a pass energy of 50 eV and high-resolution scans were made over the C 1s, O 1s, S 2p and F 1s lines using a pass energy of 15 eV. In each case, the analysis was an area-average over a region approximately 2 mm in diameter on the sample surface. Note also that in this design of system, the X-ray source is remote from the sample by approximately 1mm and so there are no thermal- or Bremsstrahlung-induced degradation effects. Charge compensation was by a low energy (5 eV) electron flood gun. The energy scale of the instrument is calibrated according to ISO standard 15472, and the intensity scale is calibrated using an in-house method traceable to the UK National Physical Laboratory. Quantification data used in this paper were obtained from the high-resolution data, rather than the survey spectra.

III. ZnO TFT as UV Photo Detectors

A. Transfer characteristics of sprayed and sputtered ZnO TFT under UV light

We have conducted UV photo detection tests on ZnO TFTs manufactured using spray and sputtered deposition methods to see the effect of UV irradiation on the TFT characteristics. Fig.1(a) shows the transfer characteristics of a ZnO TFT manufactured by spray coating and Fig.1(b) sputter coated before (black curve) and after (in blue) exposure to a UV-355 nm LED for 5 minutes at an irradiance of 0.214 mW/mm^2. In both cases, the characteristics changed dramatically and shown is the behaviour 5 minutes after light exposure, by which time the devices had saturated in terms of their electrical changes. Such behaviour is commonly known as "persistent photoconductivity." This effect can be attributed to the generation of the photo excited carriers in the degenerate level, which changes the behaviour of the ZnO from semiconducting to conducting [20].

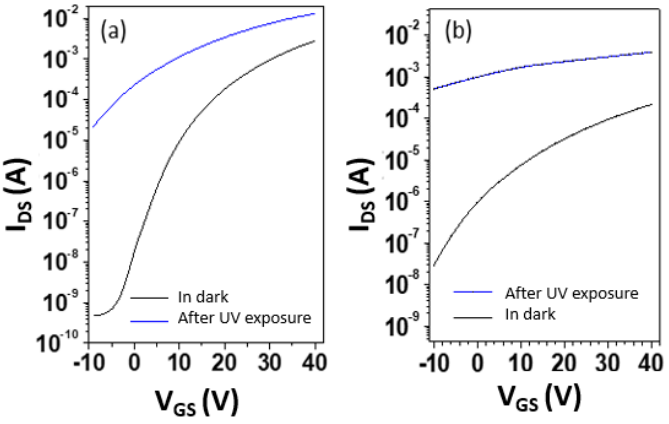

Fig. 1. Transfer curves for a ZnO TFT with the active layer deposited by (a) spray-coating, (b) sputtered before and after UV exposure for 5 minutes at an irradiance of 0.214 mW/mm^2.

The ZnO TFT performance parameters including mobility, V_{th} and on-off ratio were evaluated before and after exposure UV light. Both sets of TFTs show an overall increase in these parameters after UV exposure, however, it is more pronounced

when consider the "off-current" region (i.e. when V_{GS} <0V), owing to the increase in photoconductivity in the material. The relative change in these performance parameters is higher in case of sprayed TFTs, suggesting sprayed TFTs are more sensitive for UV irradiation.

This is quite surprising as the material is fundamentally similar; however, the structure of the spray and sputtered deposited material does differ. In particular, spray coated samples show a higher surface roughness as confirmed by AFM data (discussed later in Table 4), which will result in increased surface area which will result in higher adsorption of molecular oxygen to the film surface. In the absence of UV light, oxygen molecules can be adsorbed on the surface as negatively charged ions by capturing the free electrons from the *n*-type semiconductor, thereby create a depletion layer with low conductivity near the surface. When the sample is exposed to UV light with photon energy in the UV, it generates electron-hole pairs which result in increase in conductivity. This effect can be magnified when the surface area of ZnO is increased, which is likely to be the effect seen for the spray coated samples in Fig. 1.

Shown in Fig.2 is how the (a), (d) saturation mobility, (b), (e) OFF-current (c), (f) on-current for sprayed (left), sputtered (right) TFTs with respect to time elapsed after the UV excitation was switched off. The mobility for sprayed TFT increases with temperature and presents a slow decay time at 40 ^{0}C, however the sputtered TFTs shows similar mobility values at all temperatures of measurements. By increasing the temperature, the decay of the photo-stimulated mobility becomes faster and nearly no temperature dependence on the curves can be observed. The sprayed TFT on-current Fig.2 (c), however, presents a larger variation, with a faster decay than the carrier mobility, Fig.2 (a), at low temperature (40 ^{0}C) and almost invariant behaviour at higher temperatures (above 75 ^{0}C), indicating that the on-current increase is not only due to the increase in the carrier mobility by UV illumination, but also by the increase in the free charge carrier density in the transistor channel due to elevated temperature excitation energy. The off-current, which is a direct measure of the ZnO film conductivity, presents an even higher variation with temperature and a faster time decay, Fig.2(b), at lower temperatures. The initial value of the off-current is strongly dependent on the temperature, however, for temperatures above 75 ^{0}C, a temperature dependence cannot be observed for longer times.

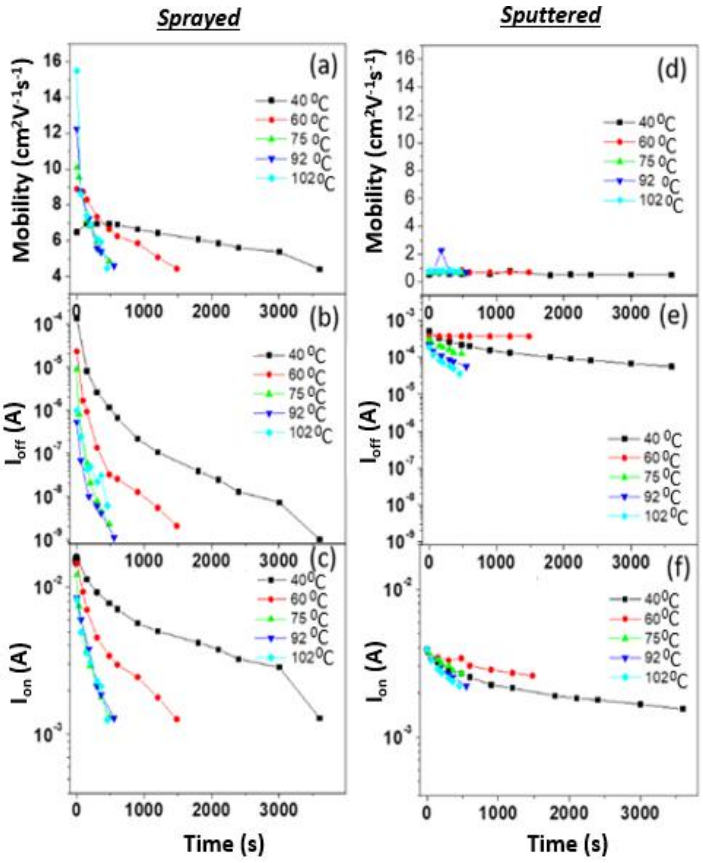

Fig. 2. Decay time of the sprayed ZnO TFT (a) mobility, (b) OFF-current, (c) Drain on-current and sputtered ZnO TFT (d) mobility, (e) off-current, (f) on-current at different temperatures.

From the observed results, we can confirm that, even though the increase in the temperature leads to an increase on the UV-stimulated carrier mobility, it is also responsible for accelerating the adsorption of the oxygen molecules to the ZnO TFT active layer, which contributes to the decrease in the carrier mobility. The TFT off-current has a faster decay time than the on-current because the contribution to the off-current comes from the conductivity of the whole ZnO layer, which has a larger area for oxygen adsorption, whereas the contribution to the on-current comes from the conductivity of the ZnO/dielectric interface, which represents a small portion of the whole ZnO film.

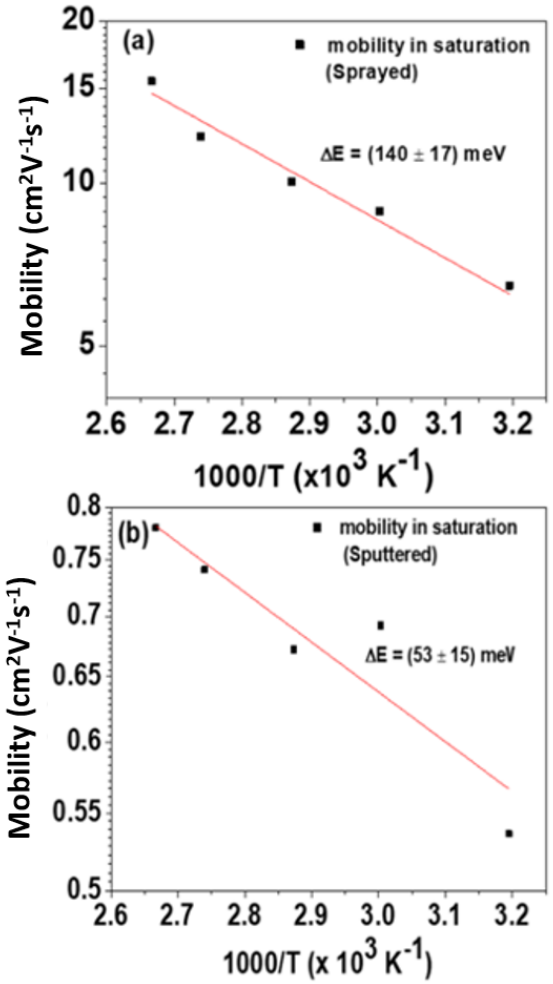

Fig. 3. Temperature dependence of the sprayed TFT mobility (a), and of sputtered ZnO TFT mobility (b) immediately after the UV light was switched off.

Fig.3 shows the temperature dependence of the sprayed TFT mobility (a), and of sputtered ZnO TFT mobility (b), immediately after the UV light was switched off. The TFT mobility increases with temperature. The density of free carriers (proportional to the TFT off current) can be expressed as equation (3), where, ΔE is the activation energy of the adsorption process.

$$n = n_0\left[1 - exp\left(-\frac{\Delta E}{k_B T}\right)\right] \qquad (3)$$

This equation was used to calculate activation energy; for sprayed TFTs, the activation energy is 140 meV and for sputtered TFTs, it is 53 meV. The temperature dependence is dominated by the thermal excitation of electrons rather than by the absorption/desorption of oxygen molecules at the surface of the ZnO film. As this process is strongly dependent of the temperature of the ZnO films, and given that the spray coated TFTs have a much higher thermal activation energy, it is not surprising that the spray coated samples are more sensitive to UV irradiation. By contrast, there is only a minor dependence of the temperature on the sputtered ZnO films, which is confirmed by the lower activation energy.

B. Responsivity and external quantum efficiency of the sprayed ZnO TFT

An important parameter to evaluate the performance of the radiation detectors is the responsivity and external quantum efficiency (EQE). Responsivity and EQE of sprayed ZnO TFTs were evaluated at three different wavelengths (λ = 355nm, 370nm, 385 nm) and shown in Fig. 4(a) and 4(b). The measurement was carried out from transfer curve at V_{DS} = 40V at room temperature in air. These properties are given, respectively, by equations (4) and (5) [21]:

$$Responsivity = \frac{{}^{I_{total}-I_{dark}}/_{A_{pt}}}{{}^{P}/_{A_{pd}}} = \frac{J_{ph}}{P} \qquad (4)$$

$$EQE = \frac{{}^{J_{ph}}/_{q}}{{}^{P}/_{h\nu}} \qquad (5)$$

Both responsivity and EQE exhibited a linear relation with wavelength for both sprayed and sputtered ZnO TFTs, as shown in Fig. 4 (a) and (b). The maximum values of the responsivity and EQE were obtained with 355nm wavelength, which are $3.65\text{x}10^4$ A/W and $1.27\text{x}10^5$ el/ph, respectively for sprayed TFTs and for sputtered TFTs values were $3.29\text{x}10^4$ A/W and $1.16\text{x}10^5$ el/ph.. Both responsivity and EQE values were increased because higher the photon energy region, the ZnO films absorb more photons and hence the number of carriers in conduction band increases, which leads to increase in the photocurrent. This value of responsivity is better as compared to another reported works. For example, Guo, *et al,* manufactured photoconductors based on transistor with mechanically exfoliated single layer of Graphene/ZnO QDs, which displayed responsivity of 10^4 A/W at UV wavelength of 325 nm and V_{DS} = 1V [22]. Dang, *et al*, showed that the maximum responsivity the ZnO Nanorods/Graphene hybrid FET under UV light at 365 nm wavelength was 3×10^5 A/W for transistors at V_{DS} = 1 V [23]. The work confirms that the use of spray coated ZnO films provides the pathway for highly sensitive UV photodetectors. Evidently the responsivity depends strongly on the type device, UV wavelength, material composition, structure and morphology as well as of the bias Voltages. However, our ZnO TFTs possess a large channel (L=400μm) and were measured at room temperature in air, which clearly highlights the promising results for responsivity and EQE.

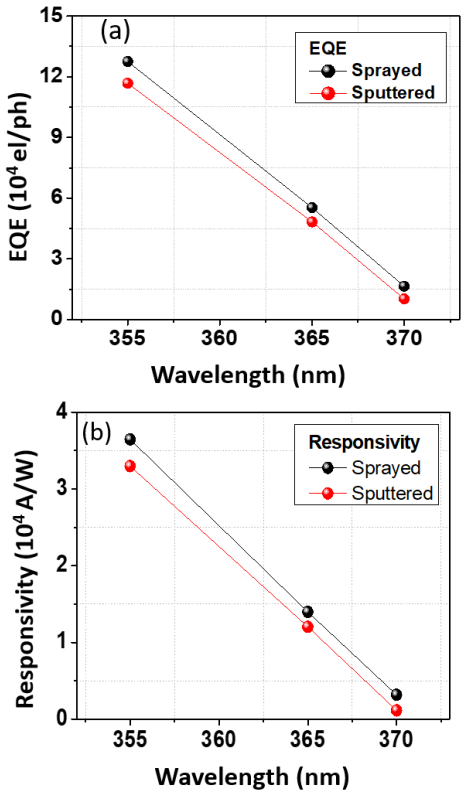

Fig. 4. (a) EQE and (b) responsivity evaluated at different wavelengths (λ = 355nm, 370nm and 385 nm)

TABLE 1. SURFACE COMPOSITION FOR SPUTTERED AND SPRAY-COATED ZnO FILMS

Element	Position [eV]	Surface concentration, atom %			
		Sputtered Films		Spray-coated films	
		As-prepared	Annealed	300 [˚C]	450 [˚C]
C 1s	284.8	39.12	27.79	22.75	22.53
O 1s	530	38.59	42.33	48.07	48.69
Zn $2p^{3/2}$	1022	22.29	29.71	29.18	28.77
Cl 2p		-	0.16	-	-

IV. XPS ANALYSIS OF ZNO FILMS

X-ray photoelectron spectroscopy (XPS) was performed on both sputtered and sprayed ZnO TFTs to see the effects of UV light on ZnO TFT photodetector. From XPS data anlysis, the samples consisted of near-pure stoichiometric ZnO with a hydrocarbon overlayer due to absorption from the environment, as is usually seen in XPS analysis of air-exposed samples. Annealing did not appear to change the chemistry or stoichiometry of the ZnO; however, it did result in a reduction in the amount of hydrocarbon contamination.If the hydrocarbon was assumed to be present as a uniform thin overlayer, then its thickness was reduced from approximately 1.75nm to approximately 1.15nm on annealing. For spray-coated films, where hydrocarbon contamination did not play an important role, annealing seemed to change slightly the sample chemistry and stoichiometry, leading to a higher amount of oxygen in metallic bonds in the crystalline lattice and a higher amount of oxygen vacancies, leading to more UV light sensitivity of sprayed TFTs.

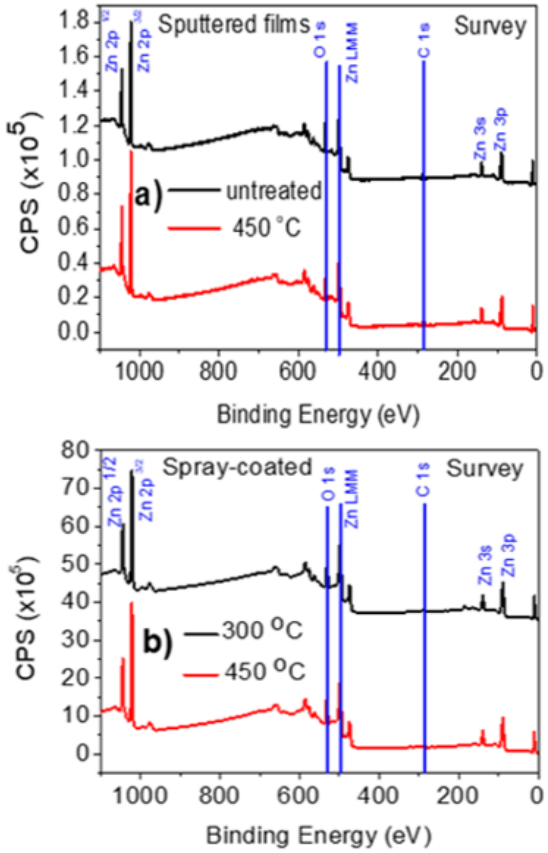

Fig. 5. XPS survey scans from sputtered (a) and spray-coated ZnO films.

XPS spectra from all samples (both sputtered and sprayed) showed strong Zn and O peaks, with C also present. The annealed sputtered sample also showed a very low level of Cl. As an example, the survey scan for the as-prepared sputtered sample is shown in Figure 5(a) and for the spray-coated films, in Figure 5(b). The results of quantification of the data are shown in Table 1.

The data shows that annealing of the sputtered films reduced the amount of surface carbon present and also reduced the ratio of oxygen to zinc from ~ 1.7 to ~ 1.4. Stoichiometric ZnO is expected to show a ratio of O/Zn of 1. The difference is probably due to preferential attenuation of the Zn $2p_{3/2}$ signal compared to the O 1s signal by the surface carbonaceous overlayer, as a consequence of the lower kinetic energy of the Zn $2p_{3/2}$ photoelectrons. To correct the measured surface compositions for the effect of the hydrocarbon overlayer, the method of Smith (2005) was applied [24]. In this method, the carbon composition is used to estimate the thickness of the

hydrocarbon contamination overlayer, the effect of a layer of this thickness on the attenuation of signals from the underlying material is estimated, and the results are re-normalised to 100 atom %. The results of applying this correction for sputtered samples are shown in Table 2.

The results show a much closer approach to the stoichiometric ZnO, as expected, but a smaller Zn content in the spray coated film, indicating a lower level of C impurities. The slight excess of O is most likely due to the presence of some carbon-bonded oxygen. Hydrocarbon contamination in spray-coated films was not so significant and the correction procedure was not applied.

TABLE 2. SURFACE COMPOSITIONS AFTER APPLICATION OF THE HYDROCARBON CONTAMINATION OVERLAYER CORRECTION

		As prepared	Annealed
	Hydrocarbon layer thickness (nm):	1.75	1.15
Element and line	O 1s	52.94	51.78
	Zn $2p^{3/2}$	47.06	48.22
Ratio O/Zn		1.13	1.07

High resolution scans over the O1s peaks (for sputtered and sprayed samples) are shown in Fig.6 also, curve-fitted to known chemical state reference data. The spectra from the sputtered films show a strong component at approximately 530.4 eV and a broader component at approximately 532 eV. The sharper component at lower binding energy is attributed to oxygen in metallic bonds (in ZnO in this case), with the broader component at higher binding energy due to oxygen in a range on unresolved carbon bonding configurations, consistent with those observed in the C 1s peak. The difference between as-prepared and annealed samples is consistent with the reduction in the hydrocarbon contamination layer (and its associated oxygen bonds) on annealing.

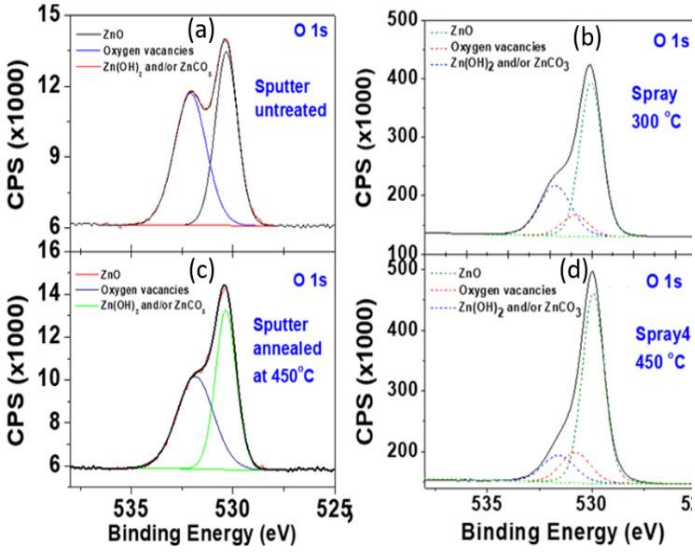

Fig. 6. (a) Sputtered untreated high-resolution spectra for O 1s, (b) sputtered annealed at 450 ^{0}C high-resolution spectra for O 1s (c) sprayed at 300 ^{0}C high-resolution spectra for O 1s (d) sprayed at 450 ^{0}C high-resolution spectra for O 1s.

TABLE 3. COMPONENT ASSIGNMENT FOR THE O 1S SPECTRA FROM THE SPRAY-COATED SAMPLES.

Component	Spray Annealed at 300 [^{0}C]		Spray Annealed at 450 [^{0}C]	
	Position	%At Concentration	Position	%At Concentration
O 1s (a)	530.04	60.81	529.93	69.69
O 1s (b)	530.80	10.47	530.79	15.40
O 1s (c)	531.75	28.73	531.58	14.91

High resolution scans over the C 1s peaks from sputtered samples are shown in Fig.7, with curve-fitted to known chemical state reference data. Both C 1s spectra show strong hydrocarbon peaks at 285.0 eV, with weaker components at approximately 286.5 eV and 289.0 eV due to C-O (hydroxyl) and COO- (surface acid groups). After annealing, there was a small drop in the relative proportion of acid groups compared to the non-annealed samples (11% of the C 1s intensity, compared to 15% of the C 1s intensity as prepared). However, any differences in chemical state after annealing were minor. Similar peaks (but less intense) were observed in spray-coated samples (HR scans not shown).

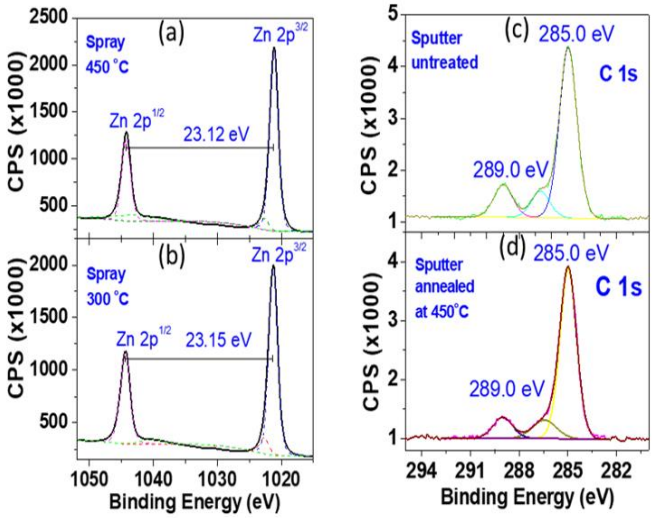

Fig. 7. (a) Zn 2p spectra for spray-coated films annealed at 450 ^{0}C, (b) Zn 2p spectra for spray-coated films annealed at 300 ^{0}C, Carbon 1s spectra for sputtered samples (c) untreated, (d) annealed at 450 ^{0}C.

Spray-coated films had much narrower O1s spectra, probably due to the longer annealing time (1 hour). The spectra were fitted considering three major contributions, as shown in Table 3. The low-energy and more intense component at 530 eV is attributed to oxygen in metallic bonds, forming crystalline ZnO. Two smaller components are observed at 530.8 eV and 531.7 eV. The higher energy component can be attributed to oxygen in ZnOH or $ZnCO_3$ bonds, since the spray coated ZnO films are formed by the pyrolysis of an organic precursor salt, zinc acetate dihydrate. The intermediate component at 530.8 eV is commonly attributed to oxygen atoms in oxygen deficient regions caused by oxygen vacancies [25]. Table 3 shows that the annealing at 450 ^{0}C increased the amount of oxygen in the crystalline lattice, simultaneously by the decrease of the amount of oxygen in ZnOH and $ZnCO_3$, which is consistent with the picture of higher conversion from zinc acetate to ZnO.

Moreover, the increase of the amount of oxygen related to oxygen vacancies for the annealed sample is in agreement with the observed improvement of the electrical properties of the films, since the n-type conductivity of ZnO can be associated to oxygen vacancies [26].

V. Atomic Force Microscopy and X-ray Diffraction of ZnO Films

AFM topography images of ZnO films prepared using spray and sputter deposition techniques are shown in in Fig.8. There is very small increase in roughness at higher annealing temperatures for both sputtered as well spray deposited films. The surface roughness of the films was evaluated in terms of root mean square (R_q), average (R_a) and peak to valley (R_{max}) and are summerised in Table 4. This small increase in roughness can be attributed to increases in grain sizes, which can be verified from the AFM images in Fig.8.

TABLE 4. SURFACE ROUGHNESS PARAMETERS OF SPRAYED AND SPUTTERED ACTIVE LAYERS OF ZNO TFTS

Anneal-ing	Sprayed Roughness Parameters			Sputtered Roughness Parameters		
T (˚C)	R_q (nm)	R_a (nm)	R_{max} (nm)	R_q (nm)	R_a (nm)	R_{max} (nm)
200	1.43	1.09	14.3	0.60	0.48	5.30
350	1.51	1.15	14.6	0.62	0.49	5.40
450	1.96	1.55	17.6	0.74	0.56	11.15

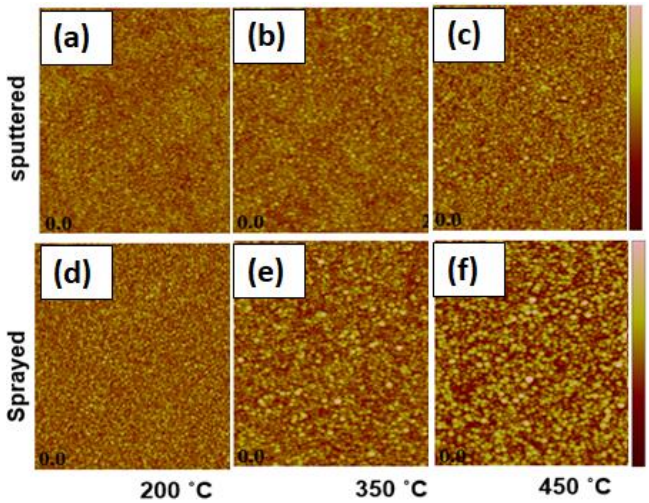

Fig. 8. (a), (b), (c) sputtered AFM topography images of sputtered and (d), (e), (f)sprayed ZnO films annealed at different temperatures shown above. Z-scale is from 0-35nm and image sizes are 8x 10µm in size

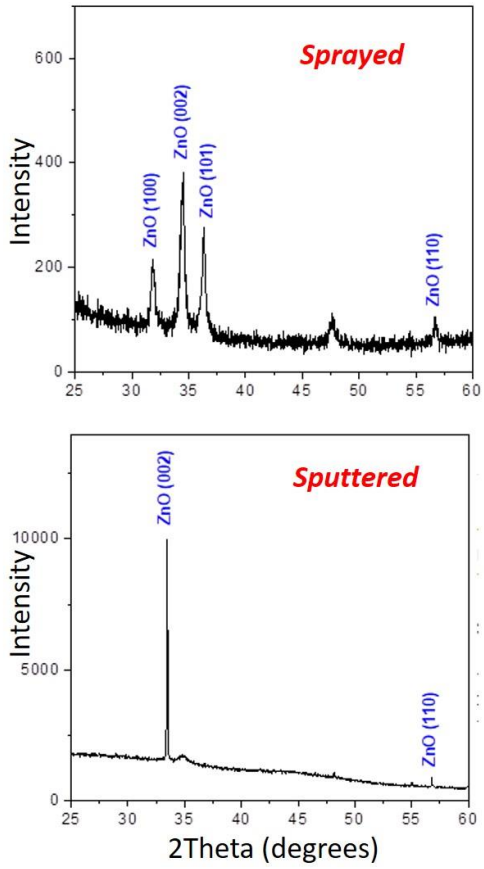

Fig. 9. XRD spectra for sprayed and sputtered ZnO films used in this work

X-ray Diffraction data (XRD) has also been used to observe the differences in crystallinity between sputtered and sprayed samples. Shown in Fig 9. are the XRD spectra for the spray and sputtered films. After analysis, it is evident that the sputtered samples present much larger grain sizes, with average crystallite sizes of 116.8 nm versus 17.8 nm for spray-coated samples. Therefore, it is possible to deduce that the surface area of the ZnO grains are much higher for spray-coated than for sputtered films.

The XRD and AFM data corroborate the sensor data from section III and confirm that the structure of the spray deposited films is rougher and the surface area is greater. It is clear that material structure plays a key role in the sensor behaviour and a more detailed study should be considered in a future work.

VI. Conclusion

The effect of UV light on ZnO photo transistors prepared by spray pyrolysis and sputtering has been investigated. It was demonstrated that sprayed ZnO TFTs are more sensitive to UV light as compared to sputtered TFTs. This is due to higher surface oxygen level in sprayed ZnO TFTs and is confirmed by XPS data. Higher surface oxygen level in sprayed ZnO TFTs can be attributed to higher surface roughness in case of sprayed which is confirmed by AFM data. This is likely to lead to an increased surface area might be responsible to higher adsorption of molecular oxygen to the film surface and this was confirmed by XPS analysis.

ACKNOWLEDGMENTS

We acknowledge the technical support from the Nanostructured Soft Materials Laboratory, LNNano-CNPEM, Brazil (XPS-23205 proposal) for XPS measurements and FAPESP-Brazil (grants # 2019/08019-9 and 2019/05620-3). JK and DK would like to thank the Welsh European Funding Office (WEFO) for funding the 2nd Solar Photovoltaic Academic Research Consortium (SPARC II)

REFERENCES

[1] K. Nomura, H. Ohta, A. Takagi, T. Kamiya, M. Hirano, and H. Hosono, "Room-temperature fabrication of transparent flexible thin-film transistors using amorphous oxide semiconductors," *Nature*, vol. 432, no. 7016, pp. 488–492, 2004.

[2] H. C. You and C. J. Wang, "Low-temperature, solution-processed, transparent zinc oxide-based thin-film transistors for sensing various solvents," *Materials (Basel).*, vol. 10, no. 3, 2017.

[3] S. Vishniakou *et al.*, "Improved Performance of Zinc Oxide Thin Film Transistor Pressure Sensors and a Demonstration of a Commercial Chip Compatibility with the New Force Sensing Technology," *Adv. Mater. Technol.*, vol. 3, no. 3, pp. 1–9, 2018.

[4] M.-H. Hsu, S.-P. Chang, S.-J. Chang, C.-W. Li, J.-Y. Li, and C.-C. Lin, "Fabrication of Zinc Oxide-Based Thin-Film Transistors by Radio Frequency Sputtering for Ultraviolet Sensing Applications," *J. Nanosci. Nanotechnol.*, vol. 18, no. 5, pp. 3518–3522, 2017.

[5] M. H. Hung *et al.*, "Ultra low voltage 1-V RFID tag implement in a-IGZO TFT technology on plastic," *2017 IEEE Int. Conf. RFID, RFID 2017*, pp. 193–197, 2017.

[6] D. Kumar,et al. "Half-volt IGZO flexible thin-film transistors with E-beam deposited Al 2 O 3 gate dielectric." *2019 IEEE International Conference on Flexible and Printable Sensors and Systems (FLEPS)*. IEEE, 2019.

[7] T.C. Gomes, D. Kumar,L. Fugikawa-Santos, N. Alves, J. Kettle, J. (2019). Optimization of the Anodization Processing for Aluminum Oxide Gate Dielectrics in ZnO Thin Film Transistors by Multivariate Analysis. *ACS combinatorial science*, *21*(5), 370-379.

[8] P. Pattanasattayavong, S. Rossbauer, S. Thomas, J. G. Labram, H. J. Snaith, and T. D. Anthopoulos, "Solution-processed dye-sensitized ZnO phototransistors with extremely high photoresponsivity," *J. Appl. Phys.*, vol. 112, no. 7, 2012.

[9] V. Q. Dang *et al.*, "High-Performance Flexible Ultraviolet (UV) Phototransistor Using Hybrid Channel of Vertical ZnO Nanorods and Graphene," *ACS Appl. Mater. Interfaces*, vol. 7, no. 20, pp. 11032–11040, 2015.

[10] J. Sun, J. Jiang, A. Lu, W. Dou, B. Zhou, and Q. Wan, "Low-voltage oxide-based TFTs self-assembled on paper substrates with tunable threshold voltage," *IEEE Trans. Electron Devices*, vol. 59, no. 2, pp. 380–384, 2012.

[11] T. Ohshima, T. Ikegami, K. Ebihara, and R. K. Thareja, "Photo-excited photonic characteristics of ZnO thin films deposited by laser ablation method," *Electr. Eng. Japan (English Transl. Denki Gakkai Ronbunshi)*, vol. 144, no. 3, pp. 1–7, 2003.

[12] L.-N. Nguyen, W.-H. Chang, C.-D. Chen, and Y.-W. Lan, "Superior phototransistors based on a single ZnO nanoparticle with high mobility and ultrafast response time," *Nanoscale Horizons*, 2019.

[13] S. K. Shaikh, V. V. Ganbavle, S. I. Inamdar, and K. Y. Rajpure, "Multifunctional zinc oxide thin films for high-performance UV photodetectors and nitrogen dioxide gas sensors," *RSC Adv.*, vol. 6, no. 31, pp. 25641–25650, 2016.

[14] S. P. Ghosh *et al.*, "Ultraviolet photodetection characteristics of Zinc oxide thin films and nanostructures," *IOP Conf. Ser. Mater. Sci. Eng.*, vol. 115, no. 1, 2016.

[15] H. Minoura, Y. Ohya, M. Kanamori, A. Kondoh, and Y. Takahashi, "Photoconductivity of Ultrathin Zinc Oxide Films," *Jpn. J. Appl. Phys.*, vol. 33, no. Part 1, No. 12A, pp. 6611–6615, 2002.

[16] S. Mansouri, R. Bourguiga, and F. Yakuphanoglu, "Analytic model for ZnO-thin film transistor under dark and UV illumination," *Curr. Appl. Phys.*, vol. 12, no. 6, pp. 1619–1623, 2012.

[17] D. A. Melnick, "Zinc oxide photoconduction, an oxygen adsorption process," *J. Chem. Phys.*, vol. 26, no. 5, pp. 1136–1146, 1957.

[18] G. Chai, O. Lupan, L. Chow, and H. Heinrich, "Crossed zinc oxide nanorods for ultraviolet radiation detection," *Sensors Actuators, A Phys.*, vol. 150, no. 2, pp. 184–187, 2009.

[19] P. Ivanoff Reyes, C. J. Ku, Z. Duan, Y. Xu, E. Garfunkel, and Y. Lu, "Reduction of persistent photoconductivity in ZnO thin film transistor-based UV photodetector," *Appl. Phys. Lett.*, vol. 101, no. 3, 2012.

[20] D. Li, L. Zhao, R. Wu, C. Ronning, and J. G. Lu, "Temperature-dependent photoconductance of heavily doped ZnO nanowires," *Nano Res.*, vol. 4, no. 11, pp. 1110–1116, 2011.

[21] J. Kettle, S. Chang, and M. Horie. "IR Sensor based on low bandgap organic photodiode with up-converting phosphor." *IEEE Sensors Journal* 15.6 (2015): 3221-3224.

[22] W. Guo, S. Xu, Z. Wu, N. Wang, and M. M. T. Loy, "Oxygen-Assisted Charge Transfer Between ZnO Quantum Dots and Graphene," *Small*, vol. 9, no. 18, pp. 3031–3036, 2013.

[23] V. Q. Dang, T. Q. Trung, and B. Hwang, "Ultrahigh Responsivity in Graphene – ZnO Nanorod Hybrid UV Photodetector," *Small*, vol. 11, no. 25, pp. 3054–3065, 2015.

[24] G. C. Smith, "Evaluation of a simple correction for the hydrocarbon contamination layer in quantitative surface analysis by XPS," *J. Electron Spectrosc. Relat. Phenom.*, vol. 1, no. 48, pp. 21–28.

[25] Y. Tu *et al.*, "Control of oxygen vacancies in ZnO nanorods by annealing and their influence on ZnO/PEDOT:PSS diode behaviour," *J. Mater. Chem. C*, vol. 6, no. 7, pp. 1815–1821, 2018.

[26] L. Liu *et al.*, "Oxygen vacancies : The origin of n -type conductivity in ZnO," vol. 235305, pp. 1–6, 2016.